

Article

Mechanical Properties Evolution of the 7B04-T74 Aluminum Alloy in the Marine Atmosphere

Ning Li ¹, Xiaojun Yan ¹, Xuerong Liu ², Lu Han ³ and Weifang Zhang ^{3,*}¹ School of Energy and Power Engineering, Beihang University, Beijing 100191, China² School of Aeronautic Science and Engineering, Beihang University, Beijing 100191, China³ School of Reliability and Systems Engineering, Beihang University, Beijing 100191, China

* Correspondence: 08590@buaa.edu.cn

Abstract: The 7xxx-series aluminum alloys are widely used in aircrafts due to their superior performance. The evolution of the mechanical properties of the aluminum alloys caused by marine atmospheric corrosion has become a research hotspot due to the increase in aircraft service time in the marine atmospheric environment. In this work, the evolution of the mechanical properties of the 7B04-T74 aluminum alloy was studied by an alternate immersion test. The surface microstructure was analyzed by SEM, EDS, XRD, and OM. The influence of the marine atmospheric corrosion on mechanical properties was studied by tensile and fatigue tests. The results show that the 7B04-T74 aluminum alloy has good corrosion resistance, as only pitting corrosion occurs in the marine atmospheric environment. The tensile properties of the 7B04-T74 aluminum alloy remained fundamentally the same before and after corrosion. The fatigue properties of the 7B04-T74 aluminum alloy were severely reduced, but the localized pitting corrosion only affected the initiation stage of the crack and had little effect on the crack propagation process.

Keywords: aluminum alloy; marine atmospheric corrosion; mechanical properties evolution



Citation: Li, N.; Yan, X.; Liu, X.; Han, L.; Zhang, W. Mechanical Properties Evolution of the 7B04-T74 Aluminum Alloy in the Marine Atmosphere. *Metals* **2022**, *12*, 2173. <https://doi.org/10.3390/met12122173>

Academic Editor: Tomáš Prošek

Received: 30 November 2022

Accepted: 14 December 2022

Published: 16 December 2022

Publisher's Note: MDPI stays neutral with regard to jurisdictional claims in published maps and institutional affiliations.



Copyright: © 2022 by the authors. Licensee MDPI, Basel, Switzerland. This article is an open access article distributed under the terms and conditions of the Creative Commons Attribution (CC BY) license (<https://creativecommons.org/licenses/by/4.0/>).

1. Introduction

The aluminum alloys have attracted considerable attention from the automotive and aerospace industries due to their excellent properties [1]. These excellent properties provide high specific strength, great workability, relatively low cost, decent thermal stability, etc., but, most importantly, they are low in density and have superior corrosion resistance [2]. As a result of these advantages, the proportion of aluminum alloys used in civil aircraft and military aircraft is over 70% and 35%, respectively [2]. Ultra-high-strength 7xxx-series aluminum alloys, as the principal aluminum alloys for aircraft structures, are widely applied in the manufacture of aircraft frame, spars, and stringers as load-bearing components, and have become one of the most prominent structural materials in this field [3,4]. As a high-strength Al-Zn-Mg-Cu-series aluminum alloy, 7B04 aluminum alloy is widely used in aviation aircrafts due to its excellent hardness, tensile strength, fracture toughness, and crack growth resistance [5–7]. The 7B04 aluminum alloy is similar in composition and mechanical properties to the 7075 aluminum alloy, but has less Fe and Si, and contains Cr for ameliorating fracture toughness and corrosion resistance [8].

Current environmental conditions around the world affect the operation of aircrafts by affecting their structural conditions, with the most common problem being corrosion, which is the result of the interaction of metallic materials with the natural environment [9]. Aluminum alloys used in aviation inevitably suffer from atmospheric corrosion when exposed to the natural environments, especially in the aircrafts serving in the humid and hot coastal and inland environments [10]. Due to the damage caused by corrosion and fatigue, such as screw rust, skin peeling, exfoliation corrosion on stringers or wing spars, corrosion fatigue cracks on the fasteners or some essential load-bearing components on the aircraft structure, the

probability of failure of aluminum alloy structures shows an obvious increasing trend with the extension of aircraft service time [11]. Thus, numerous researchers have investigated the effect on the aluminum alloys caused by atmospheric corrosion [12–14].

In order to investigate the corrosion behavior and its effect on the mechanical properties of aluminum alloys in atmospheric environments, test methods have been developed considerably around the world and a large amount of valuable data and conclusions have been obtained [15,16]. The field exposure corrosion test is the most general method in atmospheric corrosion research because its results can positively reflect the effect of the actual atmospheric environment on the materials [17]. Shi et al. [18] investigated the effect of marine atmosphere pre-corrosion and pre-fatigue on the fatigue properties of the 7085-T7452 aluminum alloy using marine atmosphere outdoor exposure tests and constant amplitude axial fatigue tests. The results showed that the fatigue properties of the 7085-T7452 aluminum alloy decreased by approximately 93% compared with the original specimens after being exposed to the actual marine atmosphere for three months. They subsequently found a similar rule for the 7075-T73 aluminum alloy [19]. Due to the enormous time and cost involved in the field exposure tests, laboratory-simulated acceleration tests have gradually become the dominant force in the study of atmospheric corrosion of metallic materials [20]. On the one hand, the corrosion resistance, the evolution of mechanical properties [21,22], and the effects arising from the environmental factors [23,24] in metals can be rapidly assessed by the results of short-term accelerated tests. On the other hand, short-term test results from the laboratory can be used to predict long-term corrosion outcomes in outdoor environments [25,26]. Cao et al. [27] studied the corrosion behavior of the 2A02 aluminum alloy with a special device that simulated the marine atmosphere. It turns out that pitting occurred close to the second phase, and the corrosion products were mainly $\text{Al}(\text{OH})_3$, Al_2O_3 , and AlCl_3 . Mishra [28] studied the consequence of pre-corrosion on mechanical properties and fatigue life of an 8011 aluminum alloy. In corrosive environments, the tensile strength and other mechanical properties of the 8011 aluminum alloy decrease extremely slowly, but the fatigue strength decreases rapidly. Cavalcante et al. [29] studied the fatigue crack propagation of 7050-T7451 and 2050-T84 aluminum alloys in air and saline environments and proved 2050-T84 aluminum alloys had superior performance due to their non-homogeneous deformation and higher corrosion resistance. Hou et al. [8] found that aggregated pits result in a nearly 80% loss of fatigue life for hole specimens of 7B04-T6 aluminum alloy exposed to a corrosion solution. However, further studies of the evolution of the mechanical properties of the aluminum alloys in the marine atmosphere using laboratory accelerated tests are needed.

Hence, in this work, the evolution of the mechanical properties of the 7B04-T74 aluminum alloy in the marine atmospheric environment were investigated by means of alternate immersion test. The surface microstructure was analyzed by SEM, EDS, XRD, and metallography detection. The tensile and fatigue tests were carried out to establish the influence of marine atmospheric corrosion on the mechanical properties of the 7B04-T74 aluminum alloy.

2. Experimental Procedures

2.1. Materials

The chemical composition of the 7B04 aluminum alloy is shown in Table 1. Rolled sheets of the 7B04 aluminum alloy were supplied by Northeast Light Alloy Co., Ltd. in China, while the heat treatment and specimen processing were performed at the Songling Processing Plant in Shenyang, China. The heat treatment technology (T74) was as follows: (1) solution treatment process: the solution temperature was maintained at 470 °C for 35 min; (2) primary aging treatment process: the aging temperature and time were 115 °C and 7 h, respectively; and (3) secondary aging treatment process: the aging temperature and time were 165 °C and 16 h, respectively.

Table 1. Chemical compositions of the 7B04-T74 aluminum alloy.

Element	Zn	Mg	Cu	Ni	Ti	Cr	Mn	Fe	Si	Al
Composition (wt%)	6.09	2.54	1.65	<0.05	0.017	0.13	0.26	0.14	0.049	Bal.

The dimension of the specimens for morphology observation is 50 mm × 50 mm × 3 mm, and its surface roughness is 1.6. The illustration of the specimens processing for the mechanical property tests is shown in Figure 1a. In order to facilitate processing, the dimension of the specimens used for the tensile test and fatigue test are basically the same, as shown in Figure 1b, which are designed according to ISO 6892-1: 2009, ISO 1099: 2006. Referring to ISO 12108: 2012, the dimension of the specimens for the fatigue crack propagation test is shown in Figure 1c. All specimens were cleaned with acetone, followed by rinsing with deionized water. After this, all specimens were dried in a draught drying cabinet for the following alternate immersion test.

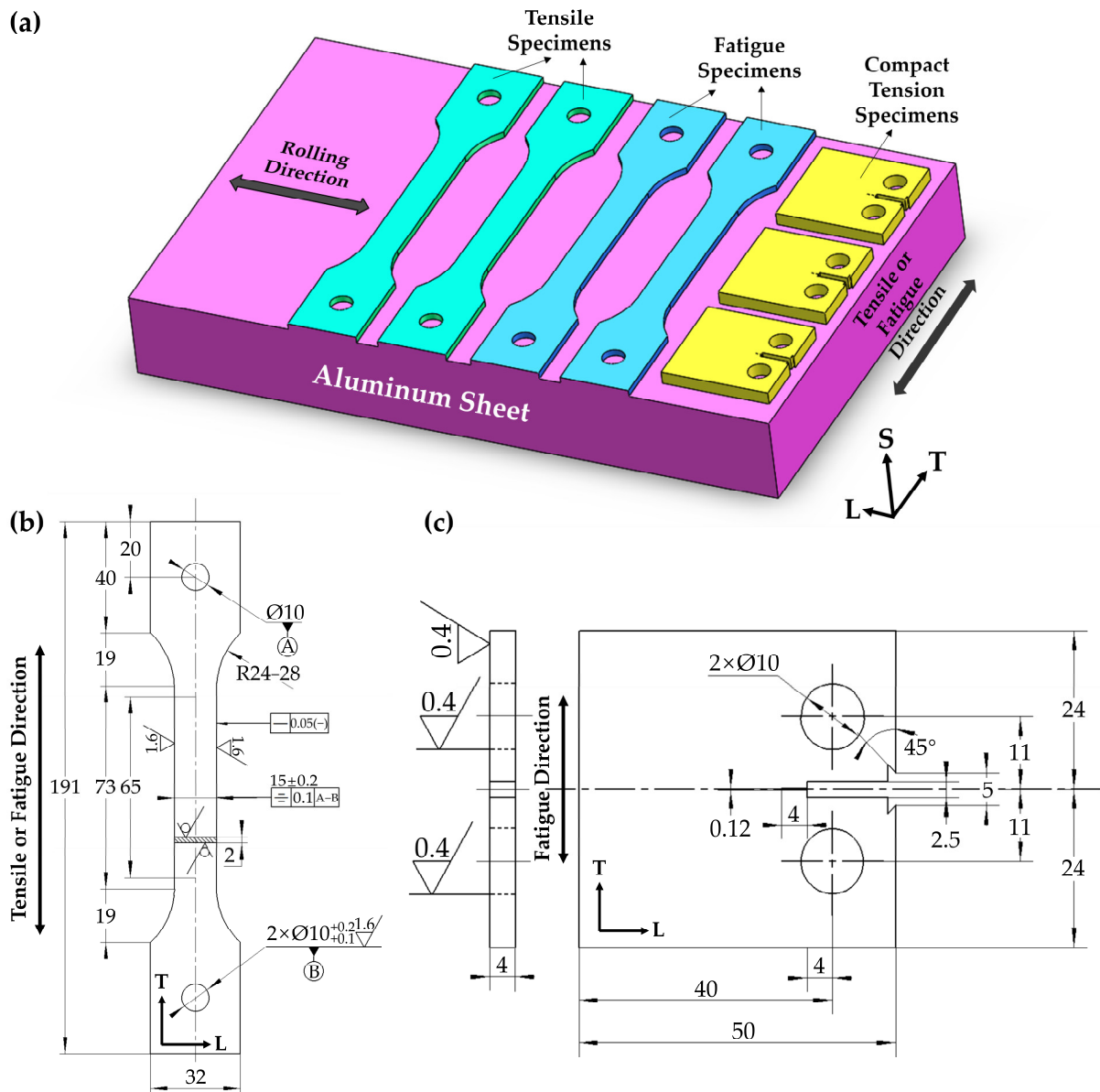


Figure 1. (a) The illustration of specimen processing and the dimensions of (b) the tensile and fatigue specimens and (c) the compact tension (CT) specimens (unit mm).

2.2. Alternate Immersion Test

The specimens were immersed in the artificial seawater for 15 min followed by exposure to air for 45 min, alternately, according to ISO 11130:2017. The chemical composition of the artificial seawater is listed in Table 2, which maintains a mass fraction of 4% of Cl^- in the seawater. A solution of 0.1 mol/L NaOH was used to modulate the pH value of the seawater to 8.2. The air temperature in the test chamber was 40 ± 1 °C while the relative humidity was $85\% \pm 1\%$. The sampling time was 48 h, 96 h, 144 h, 288 h, 432 h, and 576 h. The specimens were prepared for the follow-up testing by drying in a draught drying cabinet at 85 °C for two hours.

Table 2. Chemical compositions of the artificial seawater, g/L.

NaCl	MgCl ₂ ·6H ₂ O	Na ₂ SO ₄	CaCl ₂	KCl
37.2	16.67	6.14	1.74	1.04

2.3. Surface Morphology Observation and Composition Identification

The microstructure and morphology of the 7B04-T74 aluminum alloy were observed by scanning electron micrograph (SEM) (Zeiss Supra 55) (Carl Zeiss Meditec AG, Jena, Germany) which was equipped with energy spectrum analysis (EDS) (Oxford X-ray spectrometer) (Oxford Instruments plc, Abingdon, UK). The uncorroded specimen was converted into a metallographic specimen, which were ground, polished and corroded by the corrodent. The metallograph images were sampled by an inverted optical microscope (OM) (GX53M) (Olympus Co., Ltd., Tokyo, Japan). The composition of the corrosion product was analyzed by X-ray diffraction (XRD) (Bruker AXS D8 ADVANCE) (BRUKER AXS GmbH, Karlsruhe, Germany) with a Cu K α radiation ($\lambda = 0.15406$ nm). The tube voltage was 40 kV while the filament current was 40 mA, and the range of incident angle was 10° to 90° at the scanning rate of 5°/min. The X'Pert HighScore Plus software (v3.0, PANalytical B.V., Almelo, The Netherlands) was used to collate the X-ray diffraction data.

2.4. Mechanical Property Test

All the mechanical property tests were carried out by using a hydraulic MTS testing machine (MTS Systems Corporation, Eden Prairie, MN, USA) at room temperature after the alternate immersion test. The tensile strength, yield strength, maximum tensile stress, and elongation at break were chosen to evaluate the tensile properties, while the specimen was fractured with a loading speed of 1 mm/min. For the fatigue tests, the specimens were tested under constant amplitude cyclic loading at a maximum stress (σ_{\max}) of 271.1 MPa until fractured. For the reliability of the data, there are three parallel specimens for each test point of the tensile and fatigue tests. To further investigate the effect of marine atmospheric corrosion on the propagation of fatigue cracks in the 7B04-T74 aluminum alloys, a pre-corrosion fatigue crack propagation test was performed using the compact tension (CT) specimens. Since only the propagation of the fatigue crack is concerned, rather than the initiation of the fatigue crack, low-speed wire-cutting techniques have been used to prefabricate the crack first in order to obtain a fatigue crack that can grow stably. The CT specimens were tested under cyclic loading with mean stresses of 5, 7.5, and 10 MPa. For the fatigue crack propagation test, there were three CT specimens for each test point, which were tested at three different mean stresses, respectively. All the applied stress ratios used in the fatigue test and the fatigue crack propagation test ($R = \sigma_{\max}/\sigma_{\min}$) were 0.1, while the loading wave form was sinusoidal, and the loading frequency was 10 Hz.

3. Results and Discussion

3.1. Surface Microstructure Analysis

Figure 2a–c show the SEM morphology, EDS spectral diagram, and XRD diffraction pattern of the uncorroded specimen of the 7B04-T74 aluminum alloy, and Figure 2d is the metallographic morphology of the surface of the specimen after polishing. Through SEM

morphology, it can be observed that some inclusions were present on the surface of the specimen, as shown in Figure 2a. EDS scanning was performed on the surface of the uncorroded specimen, and it can be seen from Figure 2b that these inclusions mainly contained Cu, Fe, Mg, and other elements. On the one hand, the addition of these elements enhances the mechanical properties of the aluminum alloy [30]. On the other hand, the corrosion resistance of the aluminum alloys is affected by the second phase induced by these elements due to the different potentials of the second phase with aluminum [31]. Following the work of He [32] and Zhang [33], the inclusions are microscale intermetallic particles dominated by the $\text{Al}_7\text{Cu}_2\text{Fe}$ phase, with a slight S-phase (Al_2CuMg) and Fe-containing impurity phase (FeAl_3). Figure 2c reveals that 7B04-T74 aluminum alloy contained mainly two phases, namely α -Al and Al_3Mg_2 (β -phase) with a minor Mg_2Si phase. As shown in Figure 2d, most of the intermetallic compound particles showed uneven distribution in the grain, and a modest part of the intermetallic compound particles existed across the grain boundary.

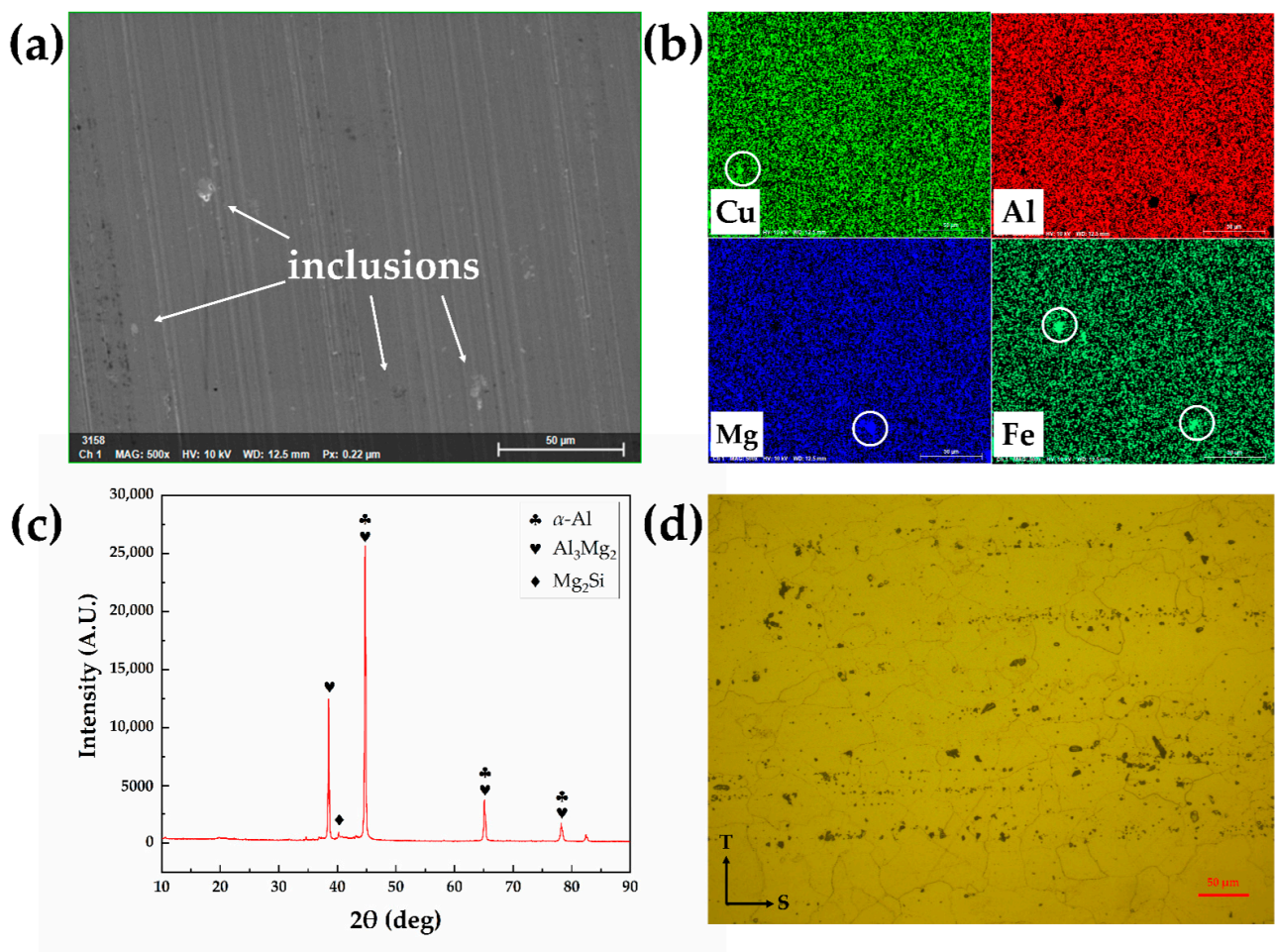


Figure 2. The SEM morphology (a), EDS spectral diagram (b), and XRD diffraction pattern (c) of the uncorroded specimen of the 7B04-T74 aluminum alloy, with the metallographic morphology (d) of the surface of the specimen after polishing.

Figure 3 shows the surface morphology of uncorroded, corroded for 48 h and 576 h specimens of the 7B04-T74 aluminum alloy. Figure 3a shows that the uncorroded specimens of the 7B04-T74 aluminum alloy with a surface roughness of 1.6 have smooth surfaces and metallic luster. As shown in Figure 3b, after 48 h of corrosion, localized pitting corrosion appeared on the surface of the specimen. The white corrosion products were deposited around the pitting corrosion regions by visual inspection. Pitting corrosion is a typical form of local corrosion in aluminum alloys. When halide ions in the environmental medium

come into contact with the surface of the aluminum alloys, the reason for pitting corrosion is commonly the breakdown of its passivation, and the possible corrosion mechanisms include penetration, adsorption, and film break [34]. The second phases contained in the aluminum alloy are the common areas for pitting corrosion [35,36]. Figure 3c shows that the specimen had lost its original metallic luster after the alternate immersion test for 576 h, and the corrosion products has increased visually around the corrosion pits. However, most of the surface of the specimen remained intact, and the corrosion was still dominated by localized pitting corrosion.

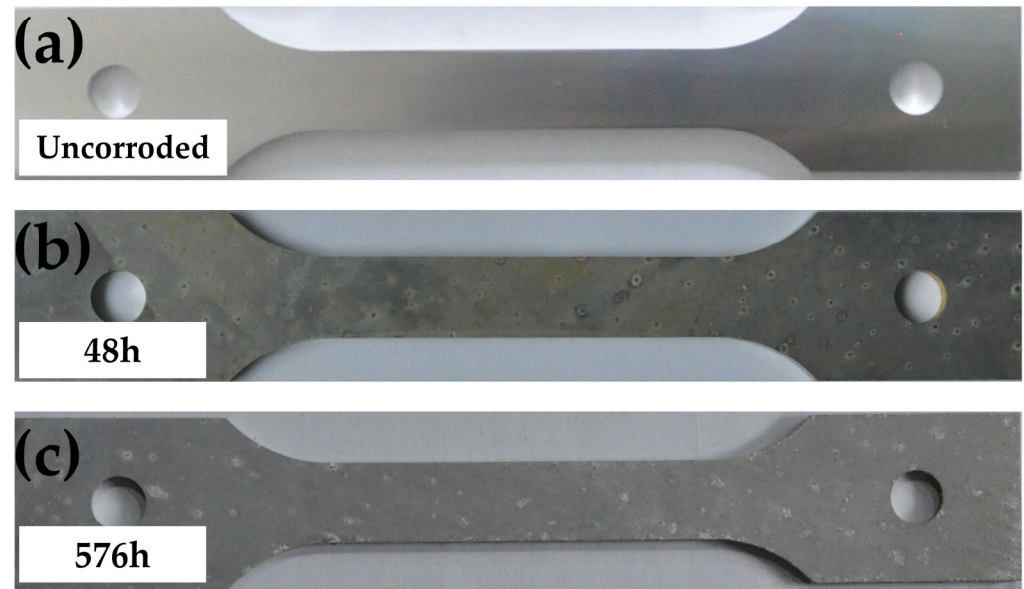


Figure 3. The surface morphology of uncorroded (a), corroded for 48 h (b), and 576 h (c) of the specimen of the 7B04-T74 aluminum alloy.

The precipitation sequence for the ultra-high-strength 7xxx-series aluminum alloys has been reported as follows: supersaturated solid solution (SSS) \rightarrow Guinier–Preston (GP) zones \rightarrow η' phase \rightarrow η phase (MgZn_2) [37]. After one-step peak aging (T6) heat treatment, GP zones and η' phase are the main hardening phases precipitated in the matrix of the 7xxx-series aluminum alloy, which makes the strength of the aluminum alloy reach a high value [38]. However, under such a heat treatment, there will be continuous distributions of precipitated phases in the grain boundaries of the aluminum alloy. Under the action of the corrosive medium, it readily develops into an anodic corrosion channel, which leads to the development of aluminum alloy from pitting corrosion to intergranular corrosion, which then considerably reduces the corrosion resistance of the aluminum alloy. In the two-step over-aging (T74) heat treatment, the first-stage low-temperature aging process is equivalent to the nucleation stage, and a large number of GP zones are generated. In the two-step high-temperature aging process, the GP zones will be transformed into η' phase, and the η' phase and η phase particles at the grain boundary will be aggregated and spheroidized, which will block the anodic corrosion channel at the grain boundary, thus greatly improving the corrosion resistance to the intergranular corrosion of the alloy [39].

Figure 4 presents the observed surface microscopic morphology of the 7B04-T74 aluminum alloy after the alternating immersion test. After 48 h of corrosion, localized pitting corrosion began to occur on the surface of specimen, as shown in Figure 4a. Except for the regions where pitting corrosion occurred, the rest of the areas maintained the integrity of the structure. From Figure 4b, the corrosion products with cracks were deposited around the pits. The cracks were caused by the water-loss effect of the corrosion products. As a result of the attack of the halogen ions, the oxide film on the surface of the aluminum alloy was broken down and the intermetallic particles exposed to the corrosion environments

tended to dissolve, thus destroying the integrity of the surface of the specimens. The pits were irregular in shape, and were accompanied by longitudinal extending cracks, as shown in Figure 4c. In Figure 4d,e, after 96 h of the atmospheric corrosion, the corrosion products attached to the pitting corrosion areas increased significantly, and a large number of tiny pits could be observed. At 144 h, the adhesion of the corrosion products could also be observed on the surface of the specimens where no obvious pitting corrosion was observed, as shown in Figure 4f. Magnification of the corrosion products shows that their morphology was essentially the same as that in Figure 4e. Corrosion developed gradually with the extension of time, resulting in the increase of the corrosion products and the size of the pits, as shown in Figure 4g,h, which are consistent with the results observed by the visual inspection. Zooming in on the pit larger in size than the others, it was observed that there was also an accumulation of the corrosion products in the interior of the pit, accompanied by cracks that extended into the interior of the matrix, as shown in Figure 4i.

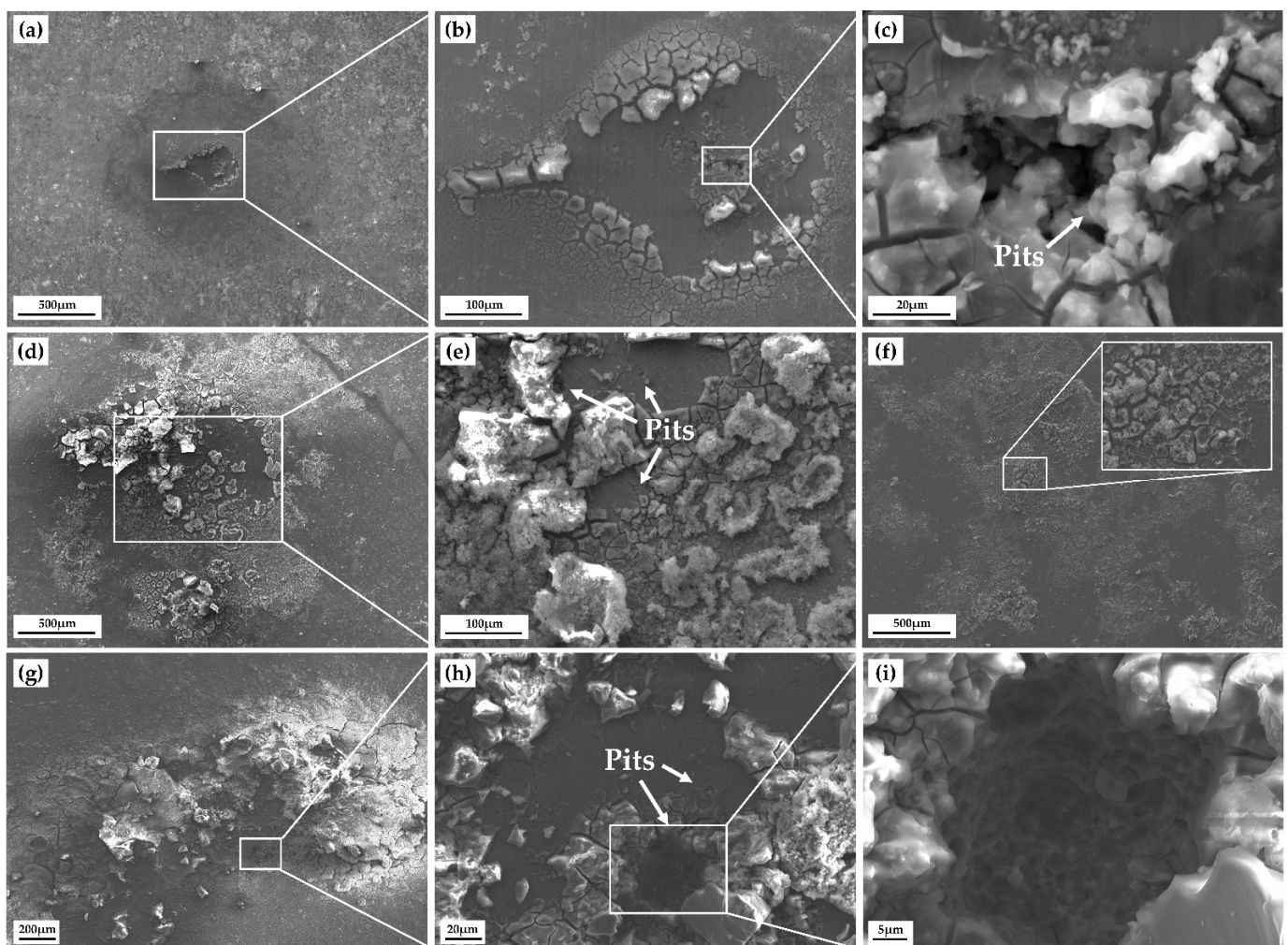


Figure 4. Surface microscopic morphology of the 7B04-T74 aluminum alloy after alternate immersion test for (a) 48 h, (d) 96 h, (f) 144 h, and (g) 576 h, where (b,c,e,h,i) are enlarged images of (a,d,g), respectively.

As discussed above, the pitting corrosion is the dominant corrosion form of the 7B04-T74 aluminum alloy in the marine atmosphere. No significant intergranular or exfoliation corrosion was observed in the specimens of the 7B04-T74 aluminum alloy after 576 h of the alternate immersion test. In the marine atmospheric conditions, the oxide film on the surface of the 7B04-T74 aluminum alloy was broken down by the Cl^- contained in the corrosive medium. Subsequently, due to the different potentials with the aluminum alloy matrix, the second phase particles, which are mainly intermetallic particles, lead to the

occurrence of electrochemical reactions, which appear in the form of pitting corrosion with cracks in morphology.

3.2. Mechanical Property Test

3.2.1. Tensile Test

Table 3 shows the tensile property parameters of the 7B04-T74 aluminum alloy after the alternate immersion test. It was clear that the tensile properties of the aluminum alloy do not alter considerably with the increase in the corrosion time. Since the 7B04-T74 aluminum alloy has no significant yield plateau, $\sigma_{0.2}$ is used to characterize its yield strength. The results of the normal distribution test applied to the data show that the mechanical properties data obtained from the first uncorroded specimen severely affect the normal distribution of the whole data. The main reason why this data is smaller than the others is that the specimen size is substandard due to low machining precision. Hence, this part of the data was removed in the subsequent analysis. Statistical analysis of the data for the remaining specimens showed that the standard deviations of yield strength, tensile strength, maximum tensile stress, and elongation at break were 3.41, 3.74, 0.17, and 0.57, respectively, indicating that marine atmospheric corrosion had little effect on the tensile properties of the 7B04-T74 aluminum alloy. Figure 5 shows the stress–strain curves of the 7B04-T74 aluminum alloy with different corrosion times. It is shown that the four curves are essentially consistent. Combined with the surface morphology analysis, it can be seen that the pitting corrosion on the surface of the 7B04-T74 aluminum alloy caused by marine atmospheric corrosion does not affect the tensile mechanical properties of the specimen.

Table 3. Tensile properties of the 7B04-T74 aluminum alloy after alternate immersion test.

Corrosion Time (h)	0		144		288		576					
Yield Strength (MPa)	443.9	476.9	486.8	478.7	478.9	482.5	479.7	474.6	476.2	481.8	477.1	479.4
Average Yield Strength (MPa)		469.2			480.1			476.8			479.4	
Tensile Strength (MPa)	501.5	533.7	544.1	536.0	536.2	538.3	536.0	530.1	532.4	539.5	534.4	535.9
Average Tensile Strength (MPa)		526.4			536.8			532.8			536.6	
Maximum Tensile Stress (kN)	22.57	24.01	24.49	24.12	24.13	24.22	24.12	23.85	23.96	24.28	24.05	24.11
Average Maximum Tensile Stress (kN)		23.69			24.16			23.98			24.15	
Elongation at Break (%)	8.41	6.86	7.49	7.16	7.97	7.37	7.45	8.14	7.34	6.97	8.83	7.48
Average Elongation at Break (%)		7.59			7.50			7.64			7.76	

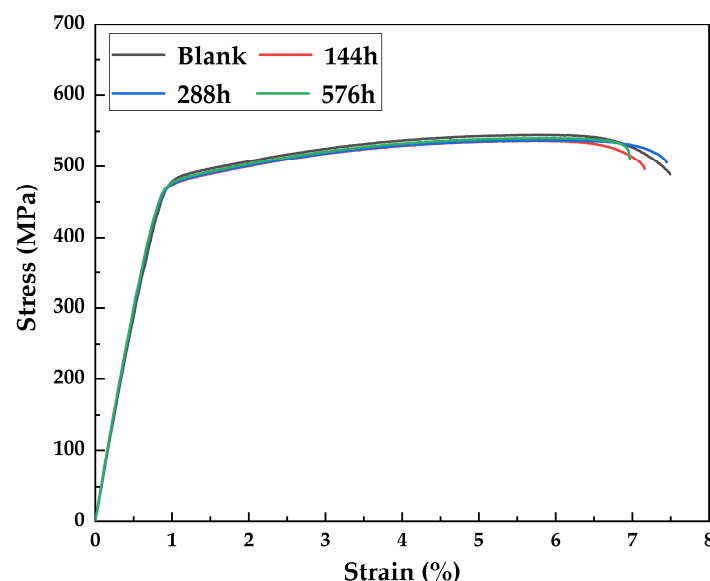


Figure 5. Stress–strain curve of the 7B04-T74 aluminum alloy after alternate immersion test.

3.2.2. Fatigue Test

Figure 6 shows the fatigue life of the 7B04-T74 aluminum alloy after the alternate immersion test. After 48 h, 96 h, 144 h, 288 h, 432 h, and 576 h of the alternate immersion test, the average fatigue life of the specimens decreased by 93.70%, 94.59%, 94.03%, 93.38%, 94.34%, and 96.00%, respectively, compared with the uncorroded state. This result indicated that the damage caused by the marine atmosphere would notably reduce the fatigue life of the 7B04-T74 aluminum alloy. This conclusion is consistent with the results of field exposure tests on similar grades of aluminum alloys [18,19]. Among them, the average fatigue life of the specimens corroded for 576 h decreased most severely, decreasing from 48.60×10^4 cycles to 1.94×10^4 cycles. Meanwhile, except for the severe degradation in the initial corrosion stage, the fatigue life still maintained a downward trend with the increasing corrosion time, but the rate of decline of the fatigue life became relatively moderate. Combined with the results of the surface microstructure observation, pitting corrosion played a great role in reducing the fatigue life of the 7B04-T74 aluminum alloy due to its pit depth. Jones [40] also demonstrated a strong correlation between the depth of the corrosion pits and the number of fracture cycles, with deeper pits generally implying fewer fracture cycles.

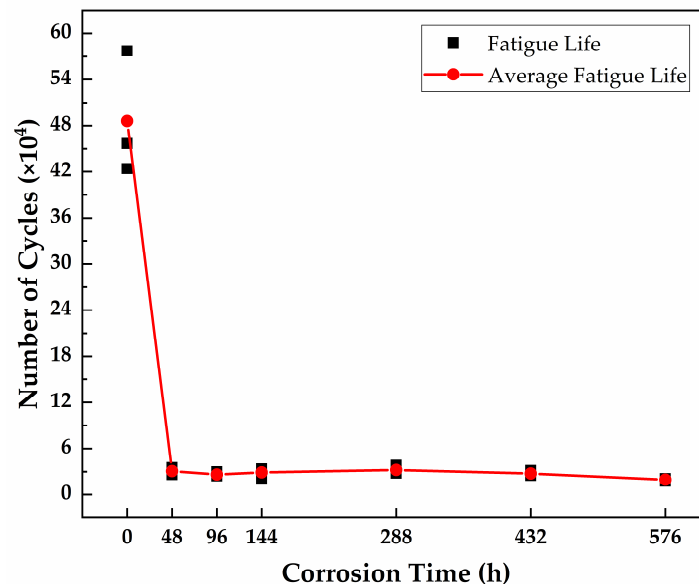


Figure 6. Fatigue life of the 7B04-T74 aluminum alloy after 576 h alternate immersion test.

In order to further investigate the effect of the marine atmospheric corrosion on fatigue crack propagation of the 7B04-T74 aluminum alloy, the fatigue crack propagation data of corroded CT specimens under different mean stresses were obtained by using the compliance method, and the corresponding crack propagating rate (da/dN) and amplitude of stress intensity factors (ΔK) were calculated from the data by the secant method. Figure 7 shows the curves of the fatigue crack propagating rate and the amplitude of stress intensity factor under different loading conditions. The da/dN vs. ΔK curve can be divided into three stages: stage I (the early stage), stage II (steady state stage), and stage III (the final stage) [41]. Due to the prefabricated crack, the curves in Figure 7 only contain the stage II and stage III. In the stage II, the fatigue crack propagating rate under constant amplitude load showed a favorable linear relationship with the amplitude of the stress intensity factor. At the same time, the curves of the specimens with different corrosion times fundamentally coincide, which proves that the fatigue crack propagation process of the 7B04-T74 aluminum alloy does not change significantly when only localized pitting corrosion occurs.

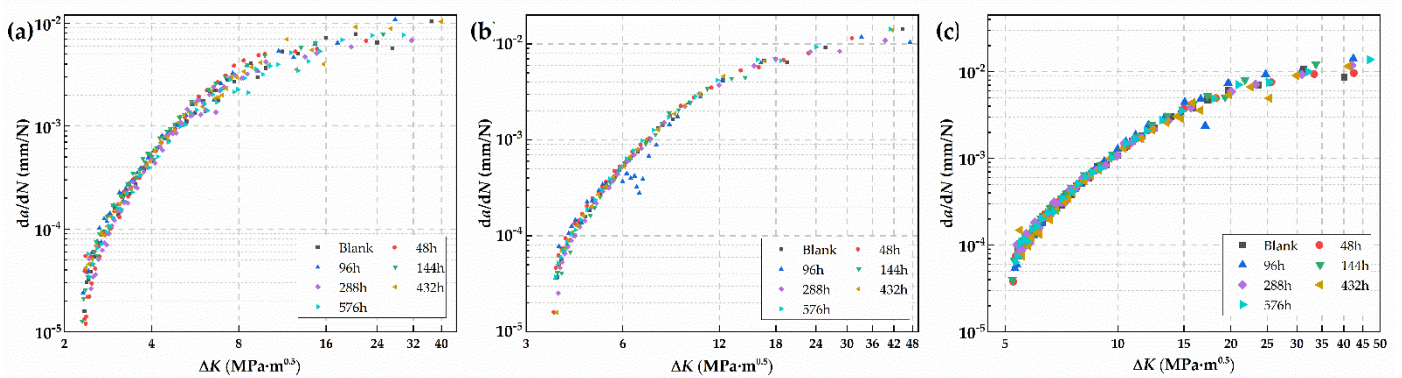


Figure 7. The curves of the fatigue crack propagating rate and the amplitude of stress intensity factor under mean stresses of (a) 5 MPa, (b) 7.5 MPa, and (c) 10 MPa.

Figure 8 shows the fatigue crack length propagation curves for different mean stress loads. The shapes of the curves at different corrosion times are essentially the same. The number of load cycles remains the same order of magnitude, which is within acceptable bounds. It was also confirmed that pits only on the surface of the 7B04-T74 aluminum alloy do not affect the propagation of fatigue cracks. As a result, the reduced fatigue life caused by the marine atmosphere of the 7B04-T74 aluminum alloy was mainly due to the effect of the pitting corrosion on the fatigue crack initiation stage. Pits accelerated the crack initiation and reduced the crack initiation life of the aluminum alloy.

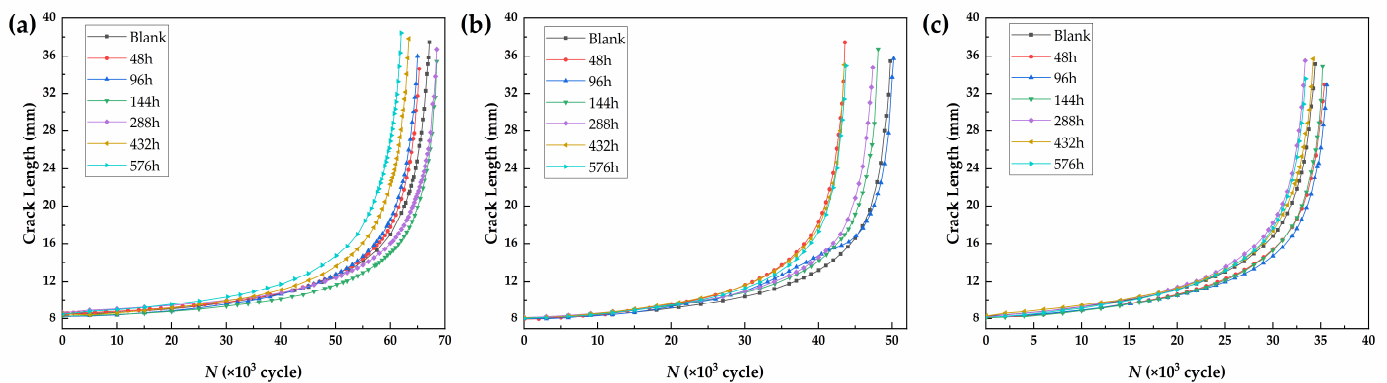


Figure 8. The curves of the fatigue crack length under mean stresses of (a) 5 MPa, (b) 7.5 MPa, and (c) 10 MPa.

To sum up, the fatigue life of the 7B04-T74 aluminum alloy is extremely sensitive to the damage caused by the marine atmospheric corrosion. When pits occur on the surface of the 7B04-T74 aluminum alloy, the fatigue life is dramatically reduced by approximately 93%. As the depth of the pit increases, the number of cycles required to fracture the specimen becomes smaller. However, the corrosion damage had no effect on the fatigue crack propagating rate of the 7B04-T74 aluminum alloy, proving that the damage mainly affected the crack initiation stage.

4. Conclusions

The evolution of the mechanical properties of the 7B04-T74 aluminum alloy in the marine atmosphere was analyzed using the alternate immersion test of 576 h, which may be useful for the evaluation of the service life and failure analysis of aluminum alloys used in aviation aircrafts in complex marine atmospheric environments. A detailed study revealed the following:

1. The 7B04-T74 aluminum alloy is sensitive to the marine atmospheric environment. Pitting corrosion occurred rapidly on the surface of the specimen at the beginning

- of the alternate immersion test. However, the pitting corrosion of the specimen did not deteriorate further as the corrosion time lengthened, and the 7B04-T74 aluminum alloy showed no significant tendency to intergranular and exfoliation corrosion;
2. After 576 h corrosion, the tensile properties of the 7B04-T74 aluminum alloy are fundamentally the same as in the non-corroded state, demonstrating that localized pitting corrosion cannot affect the tensile properties of the aluminum alloy;
 3. The fatigue properties of the 7B04-T74 aluminum alloy decreases seriously. The fatigue life of the specimens is reduced by at least 93% when pitting corrosion occurred, but this has little effect on the fatigue crack propagation rate of the specimens. The fatigue life of the specimen slowly decreases as the corrosion time increases after the pitting corrosion occurs. Pits occurring on the surface of the 7B04-T74 aluminum accelerate the crack initiation and reduce the crack initiation life of the aluminum alloy.

Author Contributions: Conceptualization, W.Z. and X.Y.; methodology, N.L. and X.L.; validation, W.Z. and X.Y.; formal analysis, N.L. and L.H.; investigation, N.L. and L.H.; resources, W.Z.; data curation, N.L. and X.L.; writing—original draft preparation, N.L.; writing—review and editing, N.L., X.L. and W.Z.; visualization, N.L. and L.H.; supervision, X.Y.; project administration, N.L.; funding acquisition, W.Z. All authors have read and agreed to the published version of the manuscript.

Funding: This research received no external funding.

Institutional Review Board Statement: Not applicable.

Informed Consent Statement: Not applicable.

Data Availability Statement: Not applicable.

Conflicts of Interest: The authors declare no conflict of interest.

References

1. Zhou, B.; Liu, B.; Zhang, S. The Advancement of 7XXX Series Aluminum Alloys for Aircraft Structures: A Review. *Metals* **2021**, *11*, 718. [[CrossRef](#)]
2. Fuente, D. Corrosion of Aluminum, Aluminum Alloys, and Composites. *Encycl. Mater. Met. Alloy.* **2022**, *1*, 160–169.
3. Koli, D.K.; Agnihotri, G.; Purohit, R. Advanced Aluminium Matrix Composites: The Critical Need of Automotive and Aerospace Engineering Fields. *Mater. Today Proc.* **2015**, *2*, 3032–3041. [[CrossRef](#)]
4. Dursun, T.; Soutis, C. Recent developments in advanced aircraft aluminium alloys. *Mater. Des.* **2014**, *56*, 862–871. [[CrossRef](#)]
5. Song, Y.H.; Zhang, T.F.; Fan, W.J.; Zhang, Y.; Yang, W.F.; Wang, A.D. Effect of the overlap ratio on surface properties of 7B04 aluminum alloy for aviation during laser derusting. *J. Mater. Res. Technol.* **2022**, *20*, 1495–1511. [[CrossRef](#)]
6. Wang, S.; Zhao, X.D.; Rong, H.S.; Wang, X.; Yang, J.; Ding, R.; Fan, W.J.; Zhang, Y. Role of *Lysinibacillus sphaericus* on aviation kerosene degradation and corrosion of 7B04 aluminum alloy. *J. Mater. Res. Technol.* **2022**, *18*, 2641–2653. [[CrossRef](#)]
7. Gao, M.; Sun, Z.H.; Yan, W.; Tang, Z.H.; Zhang, Y.N. Influence of solid particles deposition on the initial atmospheric corrosion of 7B04 aluminum alloy. *Mater. Today Commun.* **2022**, *31*, 103562. [[CrossRef](#)]
8. Hou, S.; Zhu, Y.L.; Cai, Z.H.; Wang, Y.L.; Ni, Y.H.; Du, X.K. Effect of hole cold expansion on fatigue performance of corroded 7B04-T6 aluminium alloy. *Int. J. Fatigue* **2019**, *126*, 210–220.
9. Venugopal, A.; Mohammad, R.; Koslan, M.F.S.; Sayd Bakar, S.R.; Ali, A. The Effect of Tropical Environment on Fatigue Failure in Royal Malaysian Airforce (RMAF) Aircraft Structure and Operational Readiness. *Materials* **2021**, *14*, 2414. [[CrossRef](#)]
10. Ganther, W.D.; Paterson, D.A.; Lewis, C.; Isaacs, P.; Galea, S.; Meunier, C.; Mangeon, G.; Cole, I.S. Monitoring Aircraft Microclimate and Corrosion. *Procedia Eng.* **2017**, *188*, 369–376. [[CrossRef](#)]
11. Ren, K.L.; Gao, S.W.; Liu, P.P.; Dong, Y. Influence of environmental factors on corrosion damage of aircraft structure. *Theor. Appl. Mech. Lett.* **2011**, *6*, 18–21. [[CrossRef](#)]
12. Wu, H.L.; Wu, G.; Xiang, L.; Tao, J.Q.; Zheng, Z.Y.; Sun, J.P.; Li, W.; Huang, C.Y.; Lan, X.L. Impact of Corrosion on the Degradation of the Mechanical Properties of 2195 and 2297 Al Alloys in the Marine Environment. *Metals* **2022**, *12*, 1371. [[CrossRef](#)]
13. Zhang, W.F.; Jin, T.Z.; Lou, W.T.; Li, W.L.; Dai, W. Mechanical Properties and Corrosion Behavior of 5A06 Alloy in Seawater. *IEEE Access* **2018**, *6*, 24952–24961. [[CrossRef](#)]
14. Crawford, B.R.; Loader, C.; Liu, Q.C.; Harrison, T.J.; Sharp, P.K. Can pitting corrosion change the location of fatigue failures in aircraft? *Int. J. Fatigue* **2014**, *61*, 304–314. [[CrossRef](#)]
15. Dan, Z.H.; Takigawa, S.; Muto, I.; Hara, N. Applicability of constant dew point corrosion tests for evaluating atmospheric corrosion of aluminium alloys. *Corros. Sci.* **2011**, *53*, 2006–2014. [[CrossRef](#)]
16. Dong, J.H.; Han, E.H.; Ke, W. Introduction to atmospheric corrosion research in China. *Sci. Technol. Adv. Mater.* **2007**, *8*, 559–565. [[CrossRef](#)]

17. Cai, Y.K.; Xu, Y.M.; Zhao, Y.; Ma, X.B. Atmospheric corrosion prediction: A review. *Corros. Rev.* **2020**, *38*, 299–321. [[CrossRef](#)]
18. Shi, L.X.; Xiang, L.; Tao, J.Q.; Liu, J.; Chen, Q.; Zhong, Y. Effects of Actual Marine Atmospheric Pre-Corrosion and Pre-Fatigue on the Fatigue Property of 7085 Aluminum Alloy. *Metals* **2022**, *12*, 81. [[CrossRef](#)]
19. Shi, L.X.; Xiang, L.; Tao, J.Q.; Chen, Q.; Liu, J.; Zhong, Y. Actual Marine Atmospheric Pre-Corrosion Fatigue Performance of 7075-T73 Aluminum Alloy. *Metals* **2022**, *12*, 874. [[CrossRef](#)]
20. Li, N.; Zhang, W.F.; Xu, H.; Cai, Y.K.; Yan, X.J. Corrosion Behavior and Mechanical Properties of 30CrMnSiA High-Strength Steel under an Indoor Accelerated Harsh Marine Atmospheric Environment. *Materials* **2022**, *15*, 629. [[CrossRef](#)]
21. Blücher, D.B.; Svensson, J.E.; Johansson, L.G. The influence of CO₂, AlCl₃·6H₂O, MgCl₂·6H₂O, Na₂SO₄ and NaCl on the atmospheric corrosion of aluminum. *Corros. Sci.* **2006**, *48*, 1848–1866. [[CrossRef](#)]
22. Alexopoulos, N.D.; Charalampidou, C.; Skarvelis, P.; Kourkoulis, S.K. Synergy of corrosion-induced micro-cracking and hydrogen embrittlement on the structural integrity of aluminium alloy (Al-Cu-Mg) 2024. *Corros. Sci.* **2017**, *121*, 32–42. [[CrossRef](#)]
23. Ji, Z.G.; Ma, X.B.; Zhou, K.; Cai, Y.K. An Improved Atmospheric Corrosion Prediction Model Considering Various Environmental Factors. *Corrosion* **2021**, *77*, 1178–1191. [[CrossRef](#)] [[PubMed](#)]
24. Cai, Y.K.; Zhao, Y.; Ma, X.B.; Zhou, K.; Chen, Y. Influence of environmental factors on atmospheric corrosion in dynamic environment. *Corros. Sci.* **2018**, *137*, 163–175. [[CrossRef](#)]
25. Cai, Y.K.; Xu, Y.M.; Zhao, Y.; Zhou, K.; Ma, X.B. A spatial-temporal approach for corrosion prediction in time-varying marine environment. *J. Loss. Prevent. Proc.* **2020**, *66*, 104161. [[CrossRef](#)]
26. Cai, Y.K.; Xu, Y.M.; Zhao, Y.; Ma, X.B. Extrapolating short-term corrosion test results to field exposures in different environments. *Corros. Sci.* **2021**, *186*, 109455. [[CrossRef](#)]
27. Cao, M.; Liu, L.; Yu, Z.F.; Fan, L.; Li, Y.; Wang, F.H. Electrochemical corrosion behavior of 2A02 Al alloy under an accelerated simulation marine atmospheric environment. *J. Mater. Sci. Technol.* **2019**, *35*, 651–659. [[CrossRef](#)]
28. Mishra, R.K. Study the effect of pre-corrosion on mechanical properties and fatigue life of aluminum alloy 8011. *Mater. Today Proc.* **2020**, *25*, 602–609. [[CrossRef](#)]
29. Cavalcante, T.R.F.; Pereira, G.S.; Koga, G.Y.; Bolfarini, C.; Bose Filho, W.W.; Avila, J.A. Fatigue crack propagation of aeronautic AA7050-T7451 and AA2050-T84 aluminum alloys in air and saline environments. *Int. J. Fatigue* **2022**, *15*, 106519. [[CrossRef](#)]
30. Yang, B.W.; Wang, Y.; Gao, M.Q.; Guan, R.G. The response of mechanical property to the microstructure variation of an Al-Mg alloy by adding tin element. *Mat. Sci. Eng. A-Struct.* **2021**, *825*, 141901. [[CrossRef](#)]
31. Niverty, S.; Kale, C.; Solanki, K.N.; Chawla, N. Multiscale investigation of corrosion damage initiation and propagation in AA7075-T651 alloy using correlative microscopy. *Corros. Sci.* **2021**, *185*, 109429. [[CrossRef](#)]
32. He, L.Z.; Jia, P.F.; Zhang, L.; Cui, J.Z. Evolution of secondary phases and properties of 7B04 aluminum alloy during DC homogenization. *Trans. Nonferrous Met. Soc. China* **2016**, *26*, 319–327. [[CrossRef](#)]
33. Zhang, Y.G.; Chen, Y.L.; Bian, G.X.; Zhang, Y. Electrochemical behavior and corrosion mechanism of anodized 7B04 aluminum alloy in acid NaCl environments. *J. Alloys Compd.* **2021**, *886*, 161231. [[CrossRef](#)]
34. Liang, M.X.; Melchers, R.; Chaves, I. Corrosion and pitting of 6060 series aluminium after 2 years exposure in seawater splash, tidal and immersion zones. *Corros. Sci.* **2018**, *140*, 286–296. [[CrossRef](#)]
35. Birbilis, N.; Zhu, Y.M.; Kairy, S.K.; Glenn, M.A.; Nie, J.F.; Morton, A.J.; Gonzalez-Garcia, Y.; Terry, H.; Mol, J.M.C.; Hughes, A.E. A closer look at constituent induced localised corrosion in Al-Cu-Mg alloys. *Corros. Sci.* **2016**, *113*, 160–171. [[CrossRef](#)]
36. Ma, Y.; Zhou, X.; Huang, W.; Thompson, G.E.; Zhang, X.; Luo, C.; Sun, Z. Localized corrosion in AA2099-T83 aluminum–lithium alloy: The role of intermetallic particles. *Mater. Chem. Phys.* **2015**, *161*, 201–210. [[CrossRef](#)]
37. Chen, Z.W.; Yan, K.; Ren, C.C.; Naseem, S. Precipitation sequence and hardening effect in 7A85 aluminum alloy. *J. Alloys Compd.* **2021**, *875*, 159950. [[CrossRef](#)]
38. Li, Z.H.; Xiong, B.Q.; Zhang, Y.A.; Zhu, B.H.; Wang, F.; Liu, H.W. Effects of the two-step ageing treatment on the microstructure and properties of 7B04 alloy pre-stretched thick plates. *Rare Met.* **2007**, *26*, 193–199. [[CrossRef](#)]
39. Chen, S.Y.; Chen, K.H.; Peng, G.S.; Jia, L.; Dong, P.X. Effect of heat treatment on strength, exfoliation corrosion and electrochemical behavior of 7085 aluminum alloy. *Mater. Des.* **2012**, *35*, 93–98. [[CrossRef](#)]
40. Jones, K.; Hoepfner, D.W. Prior corrosion and fatigue of 2024-T3 aluminum alloy. *Corros. Sci.* **2006**, *48*, 3109–3122. [[CrossRef](#)]
41. Liu, W.H.; Hu, Q.; Chen, Y.Q.; Tang, C.P.; Zhao, C.B.; Xiao, M.Y.; Song, Y.F. Investigation on fatigue crack propagation behaviors in the thickness direction of 2519A aluminum alloy thick plate. *Int. J. Fatigue* **2022**, *163*, 107099. [[CrossRef](#)]